

1 **Atmospheric transport and deposition of microplastics in a remote mountain catchment**

2 Steve Allen^{† a,b}, Deonie Allen^{†*a}, Vernon R. Phoenix^b, Gaël Le Roux^a, Pilar Durantez^a, Anaëlle
3 Simonneau^c, Stéphane Binet^{a,c}, Didier Galop^d

4

5 ^a EcoLab (Laboratoire Ecologie Fonctionnelle et Environnement), ENSAT, UMR-CNRS 5245,
6 Castanet Tolosan (France)

7 ^b Department of Civil and Environmental Engineering, University of Strathclyde, Glasgow, G1
8 1XQ, Scotland, UK

9 ^c ISTO, CNRS UMR 7327, Université d'Orléans, BRGM (France)

10 ^d GEODE, UMR-CNRS 5602, Université Toulouse Jean Jaurès (France)

11 [†] joint first authors (S Allen: <https://orcid.org/0000-0002-2333-6514>; D Allen:
12 <https://orcid.org/0000-0002-4038-9394>)

13 ^{*} corresponding author: deonie.allen@ensat.fr; deonia@gmail.com

14

15 **Abstract**

16 Plastic litter is an ever-increasing global issue and one of this generation's key environmental
17 challenges. Microplastics have reached oceans via river transport on a global scale, but
18 outside two mega-cities, Paris (France) and Dongguan (China), there is a lack of information
19 on atmospheric microplastic deposition or transport. Here we present the observations of
20 atmospheric microplastic deposition in a remote, pristine, mountain catchment (French
21 Pyrenees). We analyse five months of samples representing atmospheric wet and dry
22 deposition and identify fibres up to ~750 µm long and fragments ≤300µm as microplastics.
23 We document relative daily counts of 249 fragments, 73 films and 44 fibres per square
24 metre depositing on the catchment. Air mass trajectory analysis shows microplastic

25 transport through the atmosphere over a distance of up to 95km. We suggest that
26 microplastics can reach and affect remote, sparsely inhabited areas through atmospheric
27 transport.

28 Key words: microplastic, atmospheric fallout, aerosol plastic, remote area.

29 **Main text**

30 Plastic industry experts estimate global manufacture of 335 million tonnes (Mt) of plastic in
31 2016¹. Of the 335Mt worldwide, 60Mt was produced in Europe, of which ~40% is packaging
32 (short-term or single use). However, in 2016 27.1Mt was recovered as waste for recycling,
33 energy recovery (burning) or placed in landfill^{2,3}. Some plastics remain in service for up to 50
34 years, which helps explain some of the 32.9Mt discrepancy in the plastics mass balance.
35 While plastic is recognised to biodegrade very slowly, degradation to micro (5mm-1 μ m) and
36 nanoplastics (<1 μ m) does occur^{4,5}. Thus, plastic waste can start as macroplastic pieces
37 (bottles, packaging etc.) and over time degrades to microplastic (MP) particles or smaller.
38 Mattson et al.⁶ estimate 10% of created plastics enter the ocean annually, accounting for a
39 portion of the 32.9Mt plastics waste. However, this highlights questions on the fate of the
40 remaining plastic. Large amounts of macroplastic waste would be noticed in the terrestrial
41 environment, but if this waste was degraded to micro-sized particles it could evade easy
42 detection. Recent studies have identified MP on alpine river floodplains⁷ and lake sediment⁸
43 illustrating terrestrial MP occurrence, and in mega-cities as aerosol pollution⁹⁻¹². The recent
44 research on atmospheric fallout in Paris (France)⁹⁻¹¹ and Dongguan (China)¹² suggests
45 atmospheric MP conveyance and corresponding deposition. Soil/sediment/lake samples
46 provide an informative terrain-based analysis of plastic^{7,13-16} occurrence however

47 determination of atmospheric MP beyond intra-city deposition requires source specific and
48 remote atmospheric sampling.

49 This research provides unequivocal evidence of direct atmospheric fallout of MP in a remote
50 area of the Pyrenees Mountains. The Pyrenees mountainous regions are anecdotally
51 considered pristine wilderness due to limited development, difficulty of human access and
52 distance from major populations or industrial centres. The study site is located at the
53 Bernadouze meteorological station¹⁷, 42°48'14.6"N 1°25'06.8"E and 1425m a.s.l., within the
54 Vicdessos catchment and Mid-Pyrenees mountains in south-west of France (Supplementary
55 Note 1 - Detailed site description). The local vicinity is sparsely populated, without industrial,
56 commercial or large agricultural activities and is primarily used for recreational activities
57 (hiking, skiing, environmental education and scientific research). The closest local residential
58 area is a village ~6km to the south-east (Vicdessos village, population ~540¹⁸) with a
59 moderately sized town located ~25km to the north-east (Foix, population ~9,720¹⁸).

60 The presented research considers five months of atmospheric deposition collected from the
61 field site. Five samples of total atmospheric deposition (wet and dry), from two separate
62 monitoring devices, were analysed to identify if MPs are present in the remote mountain
63 catchment. Regular (monthly) sampling campaigns were proposed, however weather
64 conditions restricted site access resulting in irregular monitoring intervals (Methodology,
65 Supplementary Table 1). The objective in observing the case study atmospheric deposition
66 was to identify (1) if MPs are present in atmospheric fallout in this remote mountainous
67 location and (2) if MP are present, in what quantity, size, shape and plastic type do they
68 occur? The purpose of this study was to take steps towards discovering the extent of MP
69 atmospheric deposition in remote terrestrial locations.

70 **MP particles in the remote mountain catchment**

71 MP fragments, fibres and films were found, and confirmed (through visual microscopy
72 inspection and μ Raman analysis¹⁹) in all atmospheric deposition samples collected from the
73 field site. This illustrates that for this location there is an atmospheric MP presence. The
74 atmospheric MP deposition captured in the collectors are presented in Figure 1.

75 Figure 1 near here

76 Details of local meteorological conditions recorded at the sampling site are provided in
77 Supplementary Table 1 in conjunction with normalised MP counts (MP/m²/day) per day. The
78 meteorological record illustrates lower relative precipitation and fewer storms (rain or snow)
79 in November compared to the following months. The relative snowfall increased over the
80 monitoring period while rainfall was greatest in the January. Monthly average wind speed
81 fluctuated around 1.1(\pm 0.6)m/s with a maximum recorded wind speed of 7.1m/s in
82 December. December-March illustrate wind speeds >4m/s and the greatest relative number
83 of wind events (>2m/s and >3m/s) occurred in March. The number of >1m/s events were
84 greatest in November and March, declining to the lowest frequency in February.

85 Field sample MP counts illustrate an average daily particle deposition of 365/m²/day (\pm 69,
86 standard deviation). Sample MP counts were normalised to represent daily atmospheric
87 deposition (MP/m²/day) as site access limitations resulted in inconsistent monitoring
88 durations (November extended 12 days, December 19 days, January and March 34 days,
89 February 41 days).

90 Both rainfall and snowfall show moderate to strong significant correlations with MP count in
91 the original dataset ($r \geq 0.8$, $p < 0.05$) and to the monitoring duration (days) (Supplementary
92 Note 2). The normalised dataset presents a positive correlation to the frequency of wind

93 speeds $>1\text{m/s}$ (light air-strong wind movement) ($r>0.8$, $p<0.05$) suggesting MP transport and
94 deposition may be influenced by wind movement. The maximum rainfall intensity also
95 presents a strong positive correlation ($r>0.9$, $p<0.05$) suggesting that individual events and
96 the intensity of events may influence atmospheric MP deposition (scavenging)²⁰. While it is
97 acknowledged that the dataset is limited, the number of snowfall events also shows a
98 positive correlation with normalised MP deposition ($r\geq 0.6$, $p<0.05$). The duration (average
99 and maximum) of both rainfall and snowfall events illustrate negative correlations with MP
100 deposition ($r\leq -0.6$) suggesting event occurrence and intensity rather than duration may
101 positively influence MP deposition^{21,22}. Despite long durations (≤ 41 days) represented by the
102 samples, this preliminary dataset suggests that rain, snow and wind events may be drivers in
103 MP deposition at this site. This supports the suggestion by Dris et al.¹⁰ that precipitation
104 events may be a positive driver in atmospheric MP fallout.

105 The samples collected for the January – March monitoring period contained a visible
106 quantity of orange quartz-like fine dust. This dust presented size ($d_{50} \sim 8\mu\text{m}$), colour and
107 indicative chemical signature descriptive of Saharan dust^{23,24} (further details in
108 Supplementary Data). The fine dust, and other particulate matter potentially including some
109 MP particles, are possibly Saharan, North Africa or Iberic sourced material (or potentially
110 sourced along this trajectory)²⁵. For example, long-range transport of dust has been shown
111 by van der Does et al.²⁶ findings of ultra-giant particles ($<400\mu\text{m}$) traveling trans-oceanic up
112 to 3,500km. The distance MP can travel is currently unknown and further event-based
113 research is needed to identify source and transport vectors of atmospheric MP particles.

114 **Characteristics of MP particles**

115 Characterisation was completed following the identification guide presented by Hidalgo-Ruz
116 et al. and Noren et al.^{27,28} in conjunction with μ Raman analysis. MP particle size or length
117 was defined using the particle characterisation and count functions in ImageJ/FIJI²⁹,
118 following the method presented by Erni-Cassola et al.³⁰. The overall particle size for MP
119 particles are presented in Figure 2, with individual monitoring period sample fragment sizes
120 illustrated in Figure 2b.

121 Figure 2 near here

122 The majority of environmental MP studies that have considered particle size distribution
123 (PSD) illustrate an increasing trend in the number of finer fragments (significantly greater
124 number of MP fragments with smaller particle size)^{9,12,31}. The remote atmospheric
125 deposition samples illustrate the majority of identified MP fragments to fall $\leq 50\mu\text{m}$ and the
126 overall fragment size trend to follow previous MP particle size trends. When considered
127 relative to the monitoring period (Figure 2b) there is a slight shift in PSD curve that appears
128 to correspond to the fine dust deposition. Samples with no visible quantity of fine dust
129 (November, December) show a greater quantity of smaller fragments. The fine dust laden
130 samples show a small increase in primary fragment size (February-March). It is noted that for
131 the fine dust sample periods there are a greater number of elevated wind periods (wind
132 events $>2\text{m/s}$ and greater), higher maximum recorded wind speeds and interspersed periods
133 of calm (wind speed $<0.5\text{m/s}$) that may assist in the conveyance and deposition of the MP
134 fragments.

135 The length of plastic fibres found in the atmospheric fallout samples (Figure 2c) suggests the
136 predominant fibre lengths to be $100\text{-}200\mu\text{m}$ and $200\text{-}300\mu\text{m}$. Cai et al.¹² found the majority
137 of fibres in Dongguan to be $200\text{-}700\mu\text{m}$ in length with fibres of $\geq 4200\mu\text{m}$ (longest fibre),

138 while Dris et al.^{10,11} primarily found fibres of 200-600 μm , with the longest recorded fibre
139 \sim 5000 μm . When the scale for fibre length analysis is modified to fit previous studies, the
140 Pyrenees site fibre lengths fall predominantly between 200-700 μm (47%) (Cai et al.¹²
141 present \sim 30% in this predominant category) and 50-200 μm (30%) (Dris et al.^{10,11} illustrate a
142 higher predominant fibre length of 400-600 μm , \sim 23%). The longest fibre identified as a
143 plastic fibre in this mountain field study was 3000 μm . Film size has not specifically been
144 evaluated in previous atmospheric MP analysis so limited comparative information is
145 currently available. Films can be very thin, flat and therefore provide a greater surface area
146 for atmospheric conveyance relative to a fragment of the same mass (Figure 2a and 2d).
147 Within this mountain field study, the predominant film diameter was 50-200 μm , larger than
148 the predominant fragment size.

149 Raman spectroscopic analysis provides a verification of fragments, fibres and films as
150 plastic³¹ and characterisation of plastic type (Figure 1). The predominant plastic found in the
151 samples is polystyrene (PS) (as fragments), closely followed by polyethylene (PE). PS and PE
152 are used in many single use plastic items and in packaging material. Approximately 40% of
153 plastic demand is for plastic packaging and PS or PE products³². PS and PE are recyclable
154 products, however the European recycling rate is currently \sim 31% overall (all plastics)
155 and \sim 41% for plastic packaging (2016³²) with 3.4Mt of plastic packaging disposed in EU
156 landfill. PE has a low density compared to other plastics, 0.92-0.97g/cm²⁷ and is a common
157 film plastic (including plastic bags)³³. PS is a common packaging material having thermal
158 insulating features and the ability to provide both strong and light weight plastic products.
159 PS has a higher density than PE, 0.96-1.1g/cm^{3,27} however it is often used in a foam form for
160 packaging, insulation and protection, resulting in a significantly lowered density.
161 Polypropylene (PP) comprises 18% of the identified plastic particles (fibres primarily PP and

162 PET). PP is used in packaging, textiles and re-usable products. It is the least dense of all
163 plastics ($0.9\text{-}0.91\text{g/cm}^3$)²⁷ and due to its use in textile industry is constructed as fibres as well
164 as objects or films.

165 The composition of plastic fallout varies over the monitoring period. Initial correlation
166 analysis does not indicate any strong, significant correlations between plastic type and
167 recorded meteorology (rainfall, snowfall, wind speed or events). The complexity of the
168 plastic composition may be due to the source of plastic particles (and therefore wind
169 direction, wind strength), the occurrence of storm events and the duration of calm days
170 relative to event occurrence. The initial consideration of atmospheric MP fallout to
171 meteorological conditions does not suggest a simple meteorological mechanism driving
172 specific or preferential plastic deposition at this field site but does illustrate PS, PE and PP to
173 be the three greatest contributors to the atmospheric fallout at this location.

174 **Remote MP deposition compared to mega-city MP**

175 The MP deposition recorded at this field site equates to an average daily MP deposition of
176 $365\text{/m}^2\text{/day}$ (± 69 , particles $\geq 5\mu\text{m}$). Previous atmospheric fallout monitoring^{11,12} undertaken
177 in high density urban areas identified daily fallout of $110(\pm 96)$ and $53(\pm 38)$ particles/ $\text{m}^2\text{/day}$
178 (Paris)^{10,34} and $228(\pm 43)$ particles/ $\text{m}^2\text{/day}$ (36 MP particles/ $\text{m}^2\text{/day}$ confirmed) (Dongguan)¹².
179 Both the Paris and Dongguan studies counted and analysed particles $\geq 100\mu\text{m}$, $\geq 50\mu\text{m}$ and
180 $\geq 200\mu\text{m}$ respectively. If only $\geq 200\mu\text{m}$ particles are counted in the remote mountain field
181 samples, this equates to $40(\pm 20)$ particles/ $\text{m}^2\text{/day}$, 70% as fibres. The Pyrenees field site MP
182 deposition is comparable to the reported mega-city and suburban atmospheric MP
183 deposition despite the remote and mountainous location of notable distance from urban city
184 development or infrastructure.

185 Both the Paris and Dongguan studies primarily focused on MP fibres. If only fibres are
186 considered, the relative daily MP fibre deposition is $36(\pm 18)\text{fibres/m}^2/\text{day} \geq 100\mu\text{m}$, or
187 $28(\pm 13)\text{fibres/m}^2/\text{day} \geq 200\mu\text{m}$. This is lower but comparable to mega-city average MP
188 counts. The fibre count for the Pyrenean site for MP fibres $\geq 100\mu\text{m}$ ranges from 22-62
189 fibres/m²/day. The Paris mega-city study includes periods of lower MP deposition than seen
190 in this field study (Paris MP deposition range 2-355 MP/m²/day) potentially due to the
191 greater precipitation quantity and frequency at the Pyrenees field site compared to the Paris
192 study period. It is noted that, in concurrence with the Paris and Dongguan findings, there
193 appears to be no direct correlation between MP deposition and average daily rainfall but
194 that the occurrence of precipitation events (rain or snow) and their specific characteristics,
195 intensity and frequency, may be drivers in atmospheric fallout.

196 The Paris and Dongguan studies MP sample composition differs in plastic type as well as
197 shape to this study's findings. PS and PE form a large portion of the plastic type found in the
198 Pyrenees field site. The majority of PS particles were fragments while most fibres were PET
199 or PP. The Pyrenees field study, similarly to the Swiss floodplain findings⁷ found MP
200 composition to differ from the city atmospheric findings^{11,12}. While acknowledging the
201 different environmental compartment, there have also been several oceanic focused studies
202 that identified high counts of PS alongside PE and PP³⁵. Emerging research on the
203 degradation rate of plastics by type suggest that PS, especially EPS, is highly sensitive to
204 mechanical and UV degradation (when compared to PP and PE)⁴. Expanded PS microplastics
205 may be less dense and more easily entrained (therefore transported), and this may help
206 explain the findings at this field site. The composition of plastic waste lost to the
207 environment (not recycled or recovered) is not well documented and this, combined with

208 limited knowledge on degradation rates makes establishing the plastic waste type, shape
209 and size 'escaping' to the environment difficult to quantify or characterise.

210 **Remote atmospheric MP source and transport analysis**

211 Atmospheric MP source and transport analyses are new to MP research. Local to regional
212 transport has been considered for this field site using two methods, a simple MP settling
213 calculation and short-duration Hysplit4 back-trajectory modelling (see Methodology). Back-
214 trajectory duration is defined as ~ 2 hrs (0.1m/s settling velocity³⁶ for 600m a.g.l. Pyrenean
215 planetary boundary layer depth(PBL)³⁷) and each individual wind ($>2\text{m/s}$), rain and snow
216 event has been analysed to provide a spatial context for local MP transport. The simple MP
217 settling calculations, using MP settling velocity, event wind speed and direction and PBL
218 depth³⁷, provide basic, linear back-trajectories for MP deposited at the field site due to initial
219 entrainment or uplift and horizontal (wind) conveyance (without further mechanical or
220 convective lift). The MP source area or zone of influence defined by this method extends
221 28km north-west to south-west, along the sparsely populated Aulus-les-Bains, Ercé and
222 Massat valleys, over the Guzet-Neige ski fields and south-east along the Vicdessos valley
223 (Figure 3a-b). Wind events $>2\text{m/s}$ illustrate a local MP source area across Aulus-les-Bains and
224 the Saint-Girons valleys (42km to the north-west) and 20km to the north-east over Tarascon-
225 sur-Ariège (village populations <6000).

226 Figure 3 near here

227 Hysplit4 back-trajectory modelling allows individual event air parcels to be back-traced
228 illustrating the air parcel trajectory. Using the calculated back-trajectory duration (see
229 Methodology), models for individual rain, snow and wind events were created and collated
230 to provide event-based back-trajectory frequency maps (Figure 3c-e). These short duration

231 back-trajectories include localised updraft, convective mixing and advection, thus extending
232 the MP transport trajectories and the source area 60km to the east, 75km to the west and
233 south and 95km to the north of the site. Hysplit4 MP source areas extend into western
234 Andorra (Andorra le Vella, population ~22,250), the Spanish Pyrenees, the Saint Gaudens
235 valley, across Foix to Muret (population~24,975). However, like the MP settling calculations,
236 they still fall short of the more densely populated and industrialised areas likely to be
237 significant MP emission sources (Toulouse (population ~466,000), Barcelona (population
238 1.6million), Zaragoza (population ~661,000). This dataset does not support long-range
239 transport analysis due to the sampling time-step, however MP emissions are unlikely to be
240 limited to local sources (<100km) due to low local population density.

241 **Evidencing remote atmospheric deposition and transport**

242 This study reports atmospheric deposition of MP in a remote Pyrenean mountain location.
243 The research shows the monitored site received large numbers of MP particles (365 MP
244 particles/m²/day) in atmospheric deposition collectors over the winter period of 2017-2018.
245 The presented research illustrates the presence of MP in non-urban atmospheric fallout.
246 Analysis for this single site suggests a tentative but possibly important link between
247 precipitation (rain and/or snow), wind speed and direction to MP deposition. Initial local MP
248 trajectory assessment indicates an MP source area extending to 95km from the site,
249 reaching several towns (populations <25,000) but not the city MP emission sources such as
250 Toulouse or Zaragoza. The data cannot prove long-range transport, however air mass
251 trajectory, MP transport and settling considerations suggest MP emission sources to at least
252 be regional (>100km) given the population density within this local area. Longer-distance
253 transport modelling may be possible but requires event specific sampling and back-

254 trajectory analysis to identify the extent of this transport. It is highly recommended that
255 further monitoring and analysis be undertaken using separate dry and wet deposition
256 sampling equipment. This would advance the understanding of precipitation influence on
257 atmospheric MP deposition and wind trajectory impact on quantity and composition of
258 atmospheric MP fallout.

259

260 **Data availability.** The authors confirm that all data underlying the results presented in this
261 study are available within the Supplementary Information files and can be downloaded in
262 conjunction with this paper.

263 **References**

- 264 1. Roosevelt, C., Los Huertos, M., Garza, C. & Nevins, H. M. Marine debris in central
265 California: Quantifying type and abundance of beach litter in Monterey Bay, CA. *Mar.*
266 *Pollut. Bull.* **71**, 299–306 (2013).
- 267 2. PlasticsEurope. *Plastics – the Facts 2014 / 2015 An analysis of European plastics*
268 *production, demand and waste data.* (Plastic Recycling and Recovery Organisations
269 (EPRO), 2015).
- 270 3. PlasticsEurope. *Plastics – the Facts 2017, An analysis of the European plastics*
271 *production, demand and waste data.* (PlasticsEurope, European Association of Plastics
272 Recycling and Recovery Organisations, 2017).
- 273 4. Song, Y. K. *et al.* Combined Effects of UV Exposure Duration and Mechanical Abrasion
274 on Microplastic Fragmentation by Polymer Type. *Environ. Sci. Technol.* **51**, 4368–4376
275 (2017).

- 276 5. da Costa, J. P. Micro- and nanoplastics in the environment: Research and
277 policymaking. *Curr. Opin. Environ. Sci. Heal.* **1**, 12–16 (2018).
- 278 6. Mattsson, K., Hansson, L.-A. & Cedervall, T. Nano-plastics in the aquatic environment.
279 *Environ. Sci. Process. Impacts* **17**, 1712–1721 (2015).
- 280 7. Scheurer, M. & Bigalke, M. Microplastics in Swiss floodplain soils Microplastics in
281 Swiss floodplain soils. (2018). doi:10.1021/acs.est.7b06003
- 282 8. Hurley, R., Woodward, J. & Rothwell, J. J. Microplastic contamination of river beds
283 significantly reduced by catchment-wide flooding. *Nat. Geosci.* **11**, 251–257 (2018).
- 284 9. Gasperi, J. *et al.* Microplastics in air: Are we breathing it in? *Curr. Opin. Environ. Sci.*
285 *Heal.* **1**, 1–5 (2018).
- 286 10. Dris, R. *et al.* A first overview of textile fibers, including microplastics, in indoor and
287 outdoor environments. *Environ. Pollut.* **221**, 453–458 (2017).
- 288 11. Dris, R., Gasperi, J., Saad, M., Mirande, C. & Tassin, B. Synthetic fibers in atmospheric
289 fallout: A source of microplastics in the environment? *Mar. Pollut. Bull.* **104**, 290–293
290 (2016).
- 291 12. Cai, L. *et al.* Characteristic of microplastics in the atmospheric fallout from Dongguan
292 city, China: preliminary research and first evidence. *Environ. Sci. Pollut. Res.* **24**,
293 24928–24935 (2017).
- 294 13. Corcoran, P. L. Environmental Science Processes & Impacts Benthic plastic debris in
295 marine and fresh water environments. *Environ. Sci. Process. Impacts* **17**, 1363–1369
296 (2015).

- 297 14. Zbyszewski, M., Corcoran, P. L. & Hockin, A. Comparison of the distribution and
298 degradation of plastic debris along shorelines of the Great Lakes , North America. *J.*
299 *Great Lakes Res.* **40**, 288–299 (2014).
- 300 15. Zhang, K. *et al.* Microplastic pollution of lakeshore sediments from remote lakes in
301 Tibet plateau, China. *Environ. Pollut.* **219**, 450–455 (2016).
- 302 16. Watkins, L., McGrattan, S., Sullivan, P. J. & Walter, M. T. The effect of dams on river
303 transport of microplastic pollution. *Sci. Total Environ.* (2019).
304 doi:<https://doi.org/10.1016/j.scitotenv.2019.02.028>
- 305 17. Centre d’Etudes Spatiales de la BIOSphere (CESBIO). Donnees meteorologiques – Sud
306 Ouest Bernadouze. (2018). Available at: [http://www.cesbio.ups-](http://www.cesbio.ups-tlse.fr/data_meteo/index.php?perma=1319145390)
307 [tlse.fr/data_meteo/index.php?perma=1319145390](http://www.cesbio.ups-tlse.fr/data_meteo/index.php?perma=1319145390).
- 308 18. INSEE. Institut national de la statistique et des etudes economiques. (2018). Available
309 at: <https://www.insee.fr/fr/statistiques/3293086?geo=COM-09334>. (Accessed: 24th
310 June 2018)
- 311 19. Araujo, C. F., Nolasco, M. M., Ribeiro, A. M. P. & Ribeiro-Claro, P. J. A. Identification of
312 microplastics using Raman spectroscopy: latest developments and future prospects.
313 *Water Res.* **142**, 426–440 (2018).
- 314 20. Zwaafink, C. D. G. *et al.* Temporal and spatial variability of Icelandic dust emissions
315 and atmospheric transport. *Atmos. Chem. Phys.* 10865–10878 (2017).
316 doi:[10.5194/acp-17-10865-2017](https://doi.org/10.5194/acp-17-10865-2017)
- 317 21. Camarero, L., Bacardit, M., de Diego, A. & Arana, G. Decadal trends in atmospheric
318 deposition in a high elevation station: Effects of climate and pollution on the long-

- 319 range flux of metals and trace elements over SW Europe. *Atmos. Environ.* **167**, 542–
320 552 (2017).
- 321 22. Marticorena, B. *et al.* Mineral dust over west and central Sahel: Seasonal patterns of
322 dry and wet deposition fluxes from a pluriannual sampling (2006–2012). *J. Geophys.*
323 *Res. Atmos.* **122**, 1338–1364 (2017).
- 324 23. Morales-Baquero, R., Pulido-Villen, E. & Reche, I. Chemical signature of Saharan dust
325 on dry and wet atmospheric deposition in the south-western Mediterranean region.
326 *Tellus Ser. B* **1**, 1–12 (2013).
- 327 24. Schwikowski, M., Seibert, P., Baltensperger, U. & Gaggeler, H. W. A study of an
328 outstanding Saharan dust event at the high-alpine site Jungfraujoeh, Switzerland.
329 *Atmos. Environ.* **29**, 1829–1842 (1995).
- 330 25. Dessens, J. & Van Dinh, P. Frequent Saharan Dust Outbreaks North of the Pyrenees: A
331 sign of a climatic change? *Weather* **45**, 327–333 (1990).
- 332 26. van der Does, M., Knippertz, P., Zschenderlein, P., Giles Harrison, R. & Stuut, J.-B. W.
333 The mysterious long-range transport of giant mineral dust particles. *Sci. Adv.* **4**,
334 (2018).
- 335 27. Hidalgo-Ruz, V., Gutow, L., Thompson, R. C. & Thiel, M. Microplastics in the marine
336 environment: A review of the methods used for identification and quantification.
337 *Environ. Sci. Technol.* **46**, 3060–3075 (2012).
- 338 28. Noren, F. *Small plastic particles in Coastal Swedish waters. N-Research, KIMO Sweden*
339 (2007).
- 340 29. Schindelin, J. *et al.* Fiji: an open-source platform for biological image analysis. *Nat.*

- 341 *Methods* **9**, 676–682 (2012).
- 342 30. Erni-Cassola, G., Gibson, M. I., Thompson, R. C. & Christie-Oleza, J. A. Lost, but Found
343 with Nile Red: A Novel Method for Detecting and Quantifying Small Microplastics (1
344 mm to 20 μ m) in Environmental Samples. *Environ. Sci. Technol.* **51**, 13641–13648
345 (2017).
- 346 31. Schymanski, D., Goldbeck, C., Humpf, H. U. & Fürst, P. Analysis of microplastics in
347 water by micro-Raman spectroscopy: Release of plastic particles from different
348 packaging into mineral water. *Water Res.* **129**, 154–162 (2018).
- 349 32. European Commission. A European Strategy for Plastics in a Circular Economy. *Eur. Com.*
350 **24** (2018). doi:10.1021/acs.est.7b02368
- 351 33. Magnusson, K. *et al.* Swedish sources and pathways for microplastics to the marine
352 environment. A review of existing data. *IVL Rep.* 1–89 (2016).
- 353 34. Dris, R. *et al.* Beyond the ocean: Contamination of freshwater ecosystems with (micro-
354) plastic particles. *Environ. Chem.* **12**, 539–550 (2015).
- 355 35. Shim, W. J., Hong, S. H. & Eo, S. Chapter 1 - Marine Microplastics: Abundance,
356 Distribution, and Composition. in *Microplastic Contamination in Aquatic Environments*
357 (ed. Zeng, E. Y.) 1–26 (Elsevier, 2018). doi:https://doi.org/10.1016/B978-0-12-813747-
358 5.00001-1
- 359 36. Zender, C. S. Mineral Dust Entrainment and Deposition (DEAD) model: Description and
360 1990s dust climatology. *J. Geophys. Res.* **108**, 4416 (2003).
- 361 37. Sanchez, E., Yague, C. & Gazetner, M. A. Planetary boundary layer energetics
362 simulated from a regional climate model over Europe for present climate and climate

363 change conditions. *Geophys. Res. Lett.* **34**, (2007).

364 **Acknowledgments**

365 The data has been funded and provided by the CNRS TRAM Project, ANR-15-CE01-0008,
366 Observatoire Homme-Milieu Pyrénées Haut Vicdessos - LABEX DRIIHM ANR-11-LABX0010
367 and CESBIO. The research leading to these results has also received funding from the People
368 Programme (Marie Curie Actions) of the European Union's Seventh Framework Programme
369 (FP7/2007-2013) under REA grant agreement n. PCOFUND-GA-2013-609102, through the
370 PRESTIGE programme coordinated by Campus France. The authors would like to
371 acknowledge that this work was carried out in the CMAC National Facility, housed within the
372 University of Strathclyde's Technology and Innovation Centre, who are funded with a UKRPIF
373 (UK Research Partnership Institute Fund) capital award, SFC ref. H13054, from the Higher
374 Education Funding Council for England (HEFCE).

375 **Author contributions**

376 SA and DA designed the study, undertook all analysis and co-authored the manuscript. GLR
377 and VRF provided study design and analytical guidance and assisted preparation and revision
378 of the manuscript. PD undertook all field sampling and field protocol design, assisted in
379 sample preparation and contributed to the manuscript. AS, SB and DG provided financial
380 support and field site access that enabled this study to occur and contributed to the
381 manuscript.

382 **Corresponding Author:** The corresponding author for correspondence and requests for
383 materials relating to this paper is Dr D Allen, deonie.allen@ensat.fr.

384 **Competing interests:** The authors declare no competing interests.

385 **Figure Captions**

386 Figure 1. MP occurrence, MP type, recorded local rain and snow fall for the monitored period, wind
387 speed and wind events. See supplementary information for comment on the fragment, fibre and film
388 ratio. The types of plastics found in the atmospheric fallout derived from Raman spectroscopy
389 analysis, SpectraGryph[®] spectral analysis software and libraries⁴⁴⁻⁴⁸. The plastic types are presented
390 as abbreviations: PS (polystyrene); PE (polyethylene); PP (polypropylene); PVC (polyvinyl chloride);
391 PET (polyethylene terephthalate); other (uncharacterised).

392 Figure 2. Deposited MP characterisation. (a) and (b) illustrate the particle size distribution for the MP
393 particles identified in the monitoring period. (c) illustrates the range and predominant fibre lengths.
394 (d) illustrates the average diameter of films collected in the rain and snow collectors during the
395 monitoring periods

396 Figure 3. MP transport trajectories relative to recorded meteorology (simplistic MP settling velocity
397 trajectory calculation, Methodology Eqn.4) and Hysplit4 back-trajectory modelling. Figure 3a
398 illustrates the rain (n=165) and snow (n=186) event trajectories calculated from the maximum
399 recorded wind speed and wind direction of each storm. Figure 3b illustrates the trajectories of wind
400 events >2m/s (n=197). Figure 3c-e present the Hysplit4 back-trajectory model results for each
401 individual rain, snow or wind event >2m/s. The results have been collated and are presented as
402 trajectory frequency graphs. The wind direction data is presented in reference to local populated
403 areas to provide spatial reference.

404

405 **Methods**

406 **Field sampling and data collation**

407 The field site meteorology and sample station was visited five (5) times over the five (5) month
408 monitoring period for acquisition of samples from atmospheric fallout collectors. The sampling
409 period extended over 2017-2018 from November to March. Samples were ideally collected every 4
410 weeks but due to climatic conditions restricting access the sample periods for the five samples were
411 inconsistent (sample durations: 12, 19, 34, 41 and 34 days respectively for samples November to
412 March). Field blanks were also collected. During this period two independent atmospheric deposition
413 collectors were active at the site. The first collector was a Palmex Rain Sampler (RS1) with a sampling
414 area of 0.014m² (dia. 135mm) (constructed of UV resistant PVC and stainless steel). The second
415 collector installed and sampled from was a NILU Particulate Fallout Collector (p.n.o 9721) with a
416 sampling area of 0.03m² (dia. 200mm) (constructed of HDPE and stainless steel). Both collectors were
417 open to the atmosphere for the total period of sampling therefore all samples are a combination of
418 dry and wet atmospheric fallout. The samples collected from each atmospheric fallout collector were
419 kept separate (both during field sampling and laboratory sample preparation) thus providing a
420 duplicate sample dataset for each monitoring period.

421 During collection of the sample material (and all times when near the sampler) all persons were
422 careful to remain down-wind of the sampler, samples exposure time was kept to a minimum and
423 wherever possible cotton clothing was worn to minimise contamination. The total sample volume
424 was collected (without subsampling). Samples from the Palmex collector were decanted into clean
425 glass 2L bottles in the field capped and transported back to the laboratory. The field sample
426 container from the NILU collector was capped and transported back to the laboratory where samples
427 were decanted into clean glass 2L bottles in the laboratory 'clean room'. All decanted samples were
428 stored in a dark walk-in refrigerator (at 4 deg C) until filtration and sample processing commenced.

429 In conjunction with physical atmospheric samples wind, humidity, temperature, rainfall and snowfall
430 data was recorded at the monitoring site by the CESBIO meteorological gauging station ¹⁷. This
431 dataset provided local microclimate information at a 30 minute time-step.

432 **Sample processing preparation for MP analysis**

433 All samples (2 x 5 field samples) contained varying amounts of organic and inorganic matter including
434 biofilm and dust. To aid analysis it is necessary to remove as much of the biogenic and non-plastic
435 inorganic material as possible without damaging or losing potential plastic particles. It is also
436 necessary to remove biofilm from the plastic prior to μ Raman spectroscopy to ensure effective
437 analysis (spectra clarity). To this end, protocols were selected with the minimum physical
438 manipulation, least number of steps and the least aggressive digestion chemicals and temperatures
439 possible whilst achieving the desired results. Sample material was filtered through a 0.45 μ m PTFE
440 47mm diameter membrane (Whatman) using borosilicate laboratory glass filtration equipment and
441 vacuum dried with ethanol (96%.vol). Filters were examined and photographed under a stereo
442 microscope Olympus SZX10 with an Olympus SC30 camera attachment (and visually checked using an
443 Axiostar Plus (x50) microscope) to record as much detail of potential plastic particles as possible prior
444 to digestion. The filter was then rinsed into borosilicate glass test tubes with 10ml hydrogen peroxide
445 (H_2O_2) 30%w/w, capped with glass stoppers, and placed in a static heat block (thermomix) at 55°C for
446 7 days (no agitation). On day 8 a further 5ml of H_2O_2 30%w/w was added to each sample and the
447 sample was left for a further 7 days. H_2O_2 was chosen as the digestion medium as used by previous
448 studies ^{7,30,38,39} however given the low usage temperature of some plastics (PS=70°C PVC=60°C)⁴⁰ and
449 risk of glassing or melting at elevated temperatures, the temperature was purposefully maintained
450 below 60°C to ensure the methodology did not affect the characterisation or result in loss of
451 material.

452 On day 14 the sample was filtered onto a 0.45 μ m PTFE 47mm dia. filter membrane, rinsed with
453 250ml MilliQ (18 M Ω .cm) water and dried with ethanol (96%.vol). Filtered material was then rinsed

454 into density separation glassware with zinc chloride (technipur ZnCl₂) at 1.6g/ml density. This was
455 gently agitated (60rpm) for 7 days at room temperature (Edmund Buhler KS-15 shaker). Settled
456 material was drained away with the sediment removal valve and remaining sample filtered onto
457 0.2µm, 25mm dia. aluminium oxide filters (Andodisc™ 25). Glassware was triple rinsed onto the filter
458 with pH4 buffer. The filter was then rinsed with 250ml MilliQ water and vacuum dried with ethanol.
459 The resulting filter was then examined and photographed again to look for changes in either the
460 number of particles or particle character. Whilst it is difficult to quantify particles pre-digestion (due
461 to excessive organic/inorganic material) many of the particles photographed previously were
462 identifiable and any visible change in the material was noted, thus we are confident that the
463 protocols were sufficiently gentle to ensure minimal losses of material.

464 **Blank test**

465 Two sets of laboratory blanks were created in support of this sample preparation process. Two MilliQ
466 samples of 1L, instead of field sample material, were put through the full digestion and zinc chloride
467 separation process, resulting in two full-process blanks (following in detail the process outlined for
468 the sample preparation).

469 A further two laboratory blanks (MilliQ water samples) underwent the digestion process but were
470 filtered onto the Anodisc™ 25 filters without zinc chloride separation. The purpose of these blanks
471 was to help quantify the possible MP contamination resulting from the sampling and sample
472 preparation process.

473 Field blanks were also collected from each collector. Sample collection containers (glass) were taken
474 out on site, connected to and opened at the sample location and then returned to the laboratory.
475 These 'empty' glass containers were then thoroughly rinsed with MilliQ water and the resulting
476 water processed without zinc chloride separation, following the preparation described above.

477 The blank test resulted in a total of 6 blank samples, 2 from the complete preparation and ZnCl₂
478 process and 4 without ZnCl₂ separation (n = 6). The blank filters identified on average 3 (±1) fibres, 1
479 (±1) film and 8 (±1) fragments per filter.

480 **Visual and ImageJ/FIJI particle inspection and count**

481 All filters were visually inspected under a stereo microscope for MP particles using the identification
482 criteria published by Hidalgo-Ruz (2012), Löder and Gerdtts (2015), Norén (2007)^{27,28,41}. It is noted
483 that using visual identification alone is not recommended for MP < 500µm, a second technique (FTIR,
484 Raman) is recommended to confirm for small particles^{27,28,41,42}. Plastic particulates are visually
485 identified by their shape and colour. Plastics must have no biogenic (cellular) structure; fibres are
486 expected to have a relatively even or consistent thickness along the fibre length and illustrate three
487 dimensional bending; fragments and films are expected to have relatively homogeneous colouring
488 and illustrate a level of transparency or clarity^{28,41}. Aged plastic, such as expected in environmental
489 samples, are described by Hidalgo-Ruz (2012)²⁷ as presenting embrittled and weathered surfaces, to
490 have irregular shapes with broken and sharp edges. Weathered plastics may also show pitting. Colour
491 is also a plastic identifier^{27,41}, ranging from transparent and variations of white to bright orange,
492 blues, greens and purples through to black. It is noted that biogenic material becomes bleached
493 during the sample preparation process (H₂O₂ digestion) making plastic particulates with colour highly
494 visible and differentiated from residual (post-digestion) biogenic material.

495 An initial, indicative fragment, fibre and film count was visually undertaken for each sample using an
496 Olympus SZX10stereo microscope. Three locations of 13mm² were randomly selected and
497 investigated on each filter (two filters per sample) (random selection to minimise bias) (Peeken
498 2018). Following the visual identification methodology, a count of plastic fragments, fibres and films
499 was undertaken (n = 6 inspected areas for each sample, total of 254 MP identified). Identification
500 was conservative with a focus on obvious coloured particulates, resulting in a possible under
501 estimation overall due to limited count or testing of white and non-transparent materials.

502 All filters were then photographed using a Leica DM6000M confocal microscope with a Marzhauser
503 Scan 130/85-4mm X-Y motorised stage. Photographs were manually focused for each frame using a
504 x10 lens. Filters were photographed using the automated mosaic software (Leica proprietary
505 software) and automatically stitched to provide a multistep mosaic image for each filter. The visual
506 count was repeated on the photographs and completed using the software ImageJ. Three 13mm²
507 photographed areas of each filter were imported into ImageJ. Particle counts were undertaken using
508 the protocol defined and used by Erni-Cassola et al. (2017)³⁰ (ImageJ code provided in Erni-Cassola et
509 al (2017)³⁰ supplementary material doi: [10.1021/acs.est.7b04512](https://doi.org/10.1021/acs.est.7b04512)). A second count was undertaken
510 following the same method using a larger area (6 x 58mm²), providing a visual/ImageJ MP count for
511 50% of the AnodiscTM 25 filter surface. All identified particles (n = 1147) were sized using ImageJ (as
512 completed in Isobe et al. 2015, Imhof et al. 2016^{43,44}), providing a length, width and area appropriate
513 for particle size distribution analysis.

514 **Raman set up and analysis**

515 Confirmation of plastic presence and type was achieved by μ Raman (Horiba Scientific Xplora Plus, 50-
516 3200cm⁻¹ with a 1.5cm⁻¹ resolution, confocal imaging accuracy 0.5 μ m) confocal microscope with
517 motorised X-Y stage. μ Raman spectroscopy has been used in previous studies to confirm visual and
518 Nile Red fluorescence assisted microplastic quantification in environmental samples^{30,41,45-48} and has
519 been shown to be effective in microplastic characterisation down to 1 μ m¹⁹. Three areas of each filter
520 (6 x 13mm²) were randomly selected and analysed for total plastic presence using the 785nm laser
521 (spatial resolution of 1 μ m) and 200-2000cm⁻¹ Raman shift range. Spectra were collected using an
522 acquisition time of 15 seconds and 10 accumulations, maximum of 25% power (filter) (general
523 settings: grating of 1200gr_mm and 50 μ m split, modified to achieve effective spectra results as
524 necessary during analysis). Laser power setting were tested on plastic particles to establish the
525 strength necessary for effective spectra imaging with minimal particulate damage. Laser power of
526 25% resulted in no visible damage to the plastics and acceptable spectra delineation. Laser power of

527 50% and 100% result in damage (burning or melting) of the plastic as shown in the Supplementary
528 Note 4 – Images of Raman laser impact on plastic.

529 Each suspected plastic particle was analysed individually, resulting in a dataset of Raman shift
530 spectra's (n = 245 particulate). Each potential identified MP was analysed twice (at two unique
531 locations on the particle) to confirm the Raman spectra. Where the spectra were unclear or not
532 definitive, a third analysis was undertaken. Samples illustrating three unclear spectra were defined as
533 'not plastic'. The blank filters were tested to quantify the level of contamination (through sample
534 processing and analysis). A new Anodisc™ 25 filter was also analysed to confirm the background filter
535 spectra. The μ Raman spectral analysis provided conformation of visual identification, supporting the
536 extrapolation of visual counts to consider spatial and temporal trends.

537 **Raman Spectra analysis**

538 The open source Spectragryph software and databases⁴⁹ were used to analyse μ Raman spectral
539 results. Individual evaluation of each spectrum was completed, similar to methods of spectra analysis
540 followed in ^{45,50,51} in conjunction with ⁵² which provides a clear definition of chemical and bond
541 spectra peaks.

542 **Statistical analysis**

543 Visual and ImageJ MP counts of all filters were confirmed using μ Raman spectrography (11% of the
544 filters were analysed using μ Raman, 50% of the filters were inspected visually and with ImageJ). The
545 μ Raman confirmed count of MP ($\#/mm^2$) was extrapolated to provide an indication of the quantity of
546 MP per filter and therefore per sample. It is acknowledged that extrapolation from subsampled
547 filters does not provide a definitive MP count and ideally all MP particulates would be counted and
548 confirmed with μ Raman analysis. Due to analysis constraints complete filter analysis was not
549 possible.

550 The calculation of MP per m²/month (31 days) was calculated through a simple sum of sample area
551 MP counts, scaling using known filter and collector areas and known monitoring period durations.
552 The calculations followed the following simple equations.

553
$$\bar{X} = \frac{(\sum X_{1-n})}{n}$$
 Eqn. 1

554 \bar{X} = the average MP count for a sample area (13mm²)

555 $X_{1,2,3}$ = the MP count for a sample area 1, 2, 3 etc. (sample area = 13mm²)

556 n = sample area number (6 sample areas were investigated for each sample period)

557
$$\mu P = \left(\bar{X} \times \frac{Y}{y} \right) - \varepsilon$$
 Eqn. 2

558 μP = total MP count per filter

559 y = sample area (13mm² or 0.000013m²)

560 Y = total filter area (346 mm² or 0.0003m²)

561 ε = sampling error, the number of MP particulates found on the blank samples

562

563
$$MP = \left(\mu P \times \frac{1}{a} \right) / d$$
 Eqn. 3

564 MP = MP count per m² / day

565 a = sample area of the atmospheric collector (m²)

566 d = duration of the sampling period (days)

567 The quantity of MP/filter is accepted to be representative of the atmospheric deposition for the
568 monitoring period relative to the collection area (Palmex collector = 0.014m², NILU collector =
569 0.03m²). Provision of MP quantity/m² has been previously published and accepted as a method
570 supporting comparison of multiple studies results⁸. Therefore, the results per monitoring period
571 were normalised for 1 day time period (for comparison to Dris et al.¹¹ and Cai et al.¹²) and 1 metre
572 square area using the known collector surface areas. The two collectors provide replicate samples for

573 each sample period and therefore were treated as such. Thus, two independent samples were
574 collected for each sample period, providing 2 Anodisc™ 25 filters, with a total of 6 randomly selected
575 areas analysed for MP resulting a per monitoring period n= 6.

576 Statistical analysis of the MP counts and characteristics has been purposefully kept to a minimum
577 due to the dataset duration (5 monitoring periods) and the single site case study constraints (it is not
578 considered appropriate to generalise from a single case study), the study is presented as a first
579 indication and presentation of remote MP presence only). Simple correlation analysis between
580 particle counts and meteorological data was completed using R Studio (R version 3.4.1) software and
581 standard significance (p-value), Pearson and Spearman correlation tests used appropriate to the data
582 (CRAN packages hydroGOF, Hmisc, Performance Analytics and subsidiaries).

583 **Bias**

584 Use of a non-automated system in particle counting and analysis will induce a level of human bias in
585 the results. To reduce the potential human bias in the results due to lack of automation, random
586 sampling has been employed on all filter counting and μ Raman analysis site selection. MP visual,
587 ImageJ and μ Raman analysis has been undertaken in triplicate on all filters to further limit bias and
588 uncertainty in the results. MP identification was completed following an identification protocol that
589 was consistently employed on all areas analysed. The identification protocol was conservative, any
590 particles that did not meet visual identification protocol as described by Hidalgo-Ruz et al.²⁷ and
591 Norén²⁸ and or did not provide a clear Raman plastic signature were discounted from the analysis to
592 limit mis-identification and bias.

593 **Local transport trajectory and source area assessment**

594 The recorded wind, rain and snow meteorological data was used to support a local MP transport
595 assessment and to help consider potential source and trajectories of MP relative to the field site. The
596 simple numerical assessment of distance and transport duration of MP particles relative to rainfall
597 events, snowfall events and wind occurrences (events) were calculated using the known field site

598 elevation, upper elevation of MP entrainment³⁷, wind speed and assumed settling velocity³⁶ (based
599 on 25µm dust particle). Once elevated, it was assumed that no further meteorological updraft or
600 conveyance assistance (other than recorded horizontal wind speed and direction) influenced the MP
601 (to provide a simplified assessment of possible MP transport).

$$602 \quad \text{distance} = \frac{\text{back - trajectory duration}}{\text{wind speed}} \quad \text{Eqn. 4}$$

603 *distance* = potential horizontal trajectory of MP (m)

604 *back-trajectory duration* = the duration MP is airborne (sec); calculated as maximum elevation (600m
605 a.g.l.)³⁷ / settling velocity (0.1 m/s)³⁶

606 *wind speed* = maximum recorded wind speed (at the meteorological station) during each rain, snow
607 or wind event (m/s)

608 The wind direction recorded for the rain, snow and wind events were used in conjunction with the
609 calculated horizontal transport distances to create event specific wind rose maps to spatially
610 illustrate the local MP trajectories. It is acknowledged that this is a highly simplified assessment of
611 potential horizontal transport trajectories and does not take into account the complex atmospheric
612 dynamics of mountain terrain or atmospheric mixing. However, it does provide a first simplified
613 assessment of local MP transport.

614 **HYSPLIT4 analysis**

615 The open source modelling software HYSPLIT^{53,54} was used to model the back trajectory of air parcel
616 movement from the field site during the five monitoring periods. HYSPLIT version 4 (HYSPLIT4) was
617 used to download and model global wind/atmospheric meteorology data provided by NOAA (Global
618 Data Assimilation System data) (similarly used in⁵⁵⁻⁵⁷). Each rainfall (n=165), snowfall (n=186) and
619 wind event >2m/s (n=197) were individually modelled with the back-trajectory duration defined
620 above (Eqn. 4). The multiple individual trajectories were then collated to create a frequency chart of

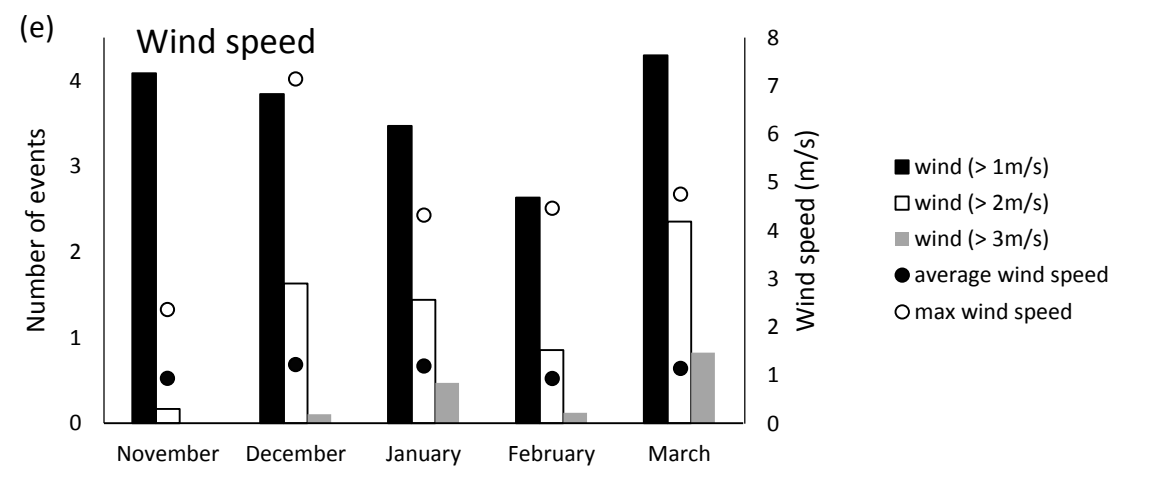
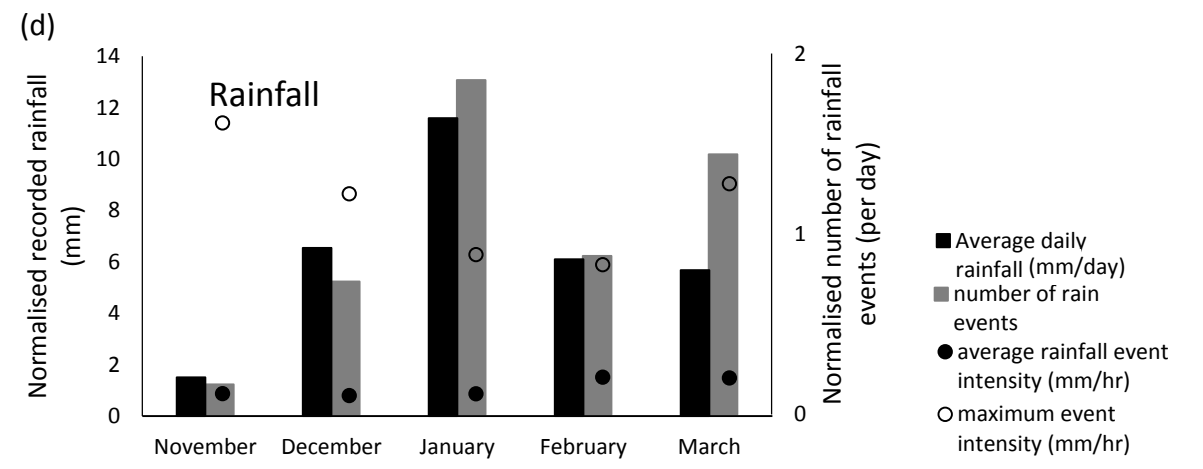
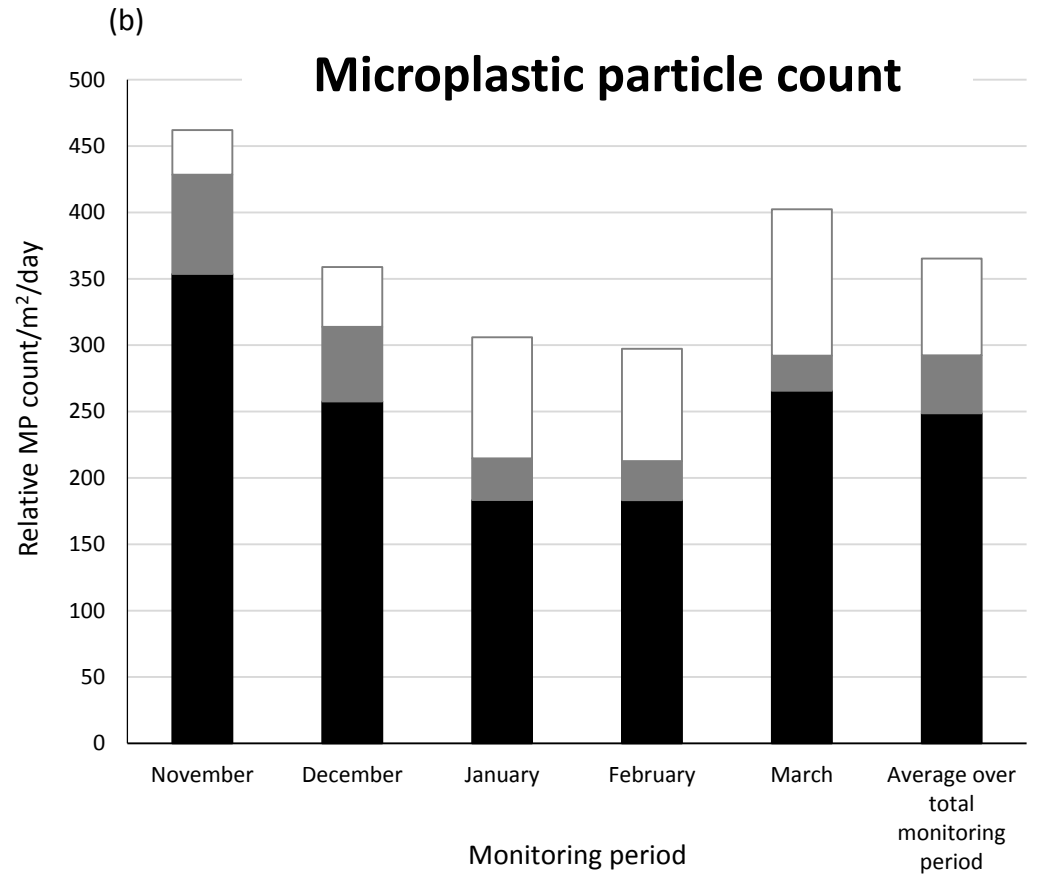
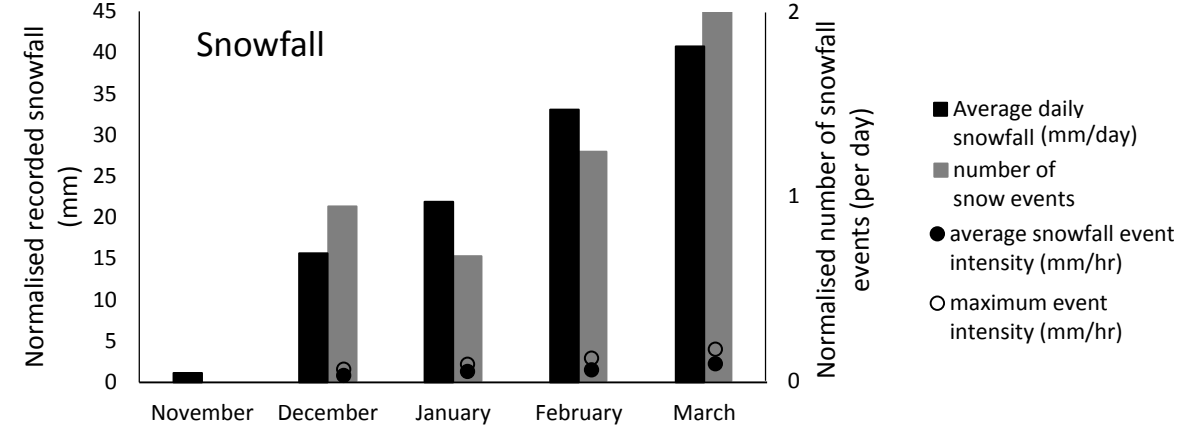
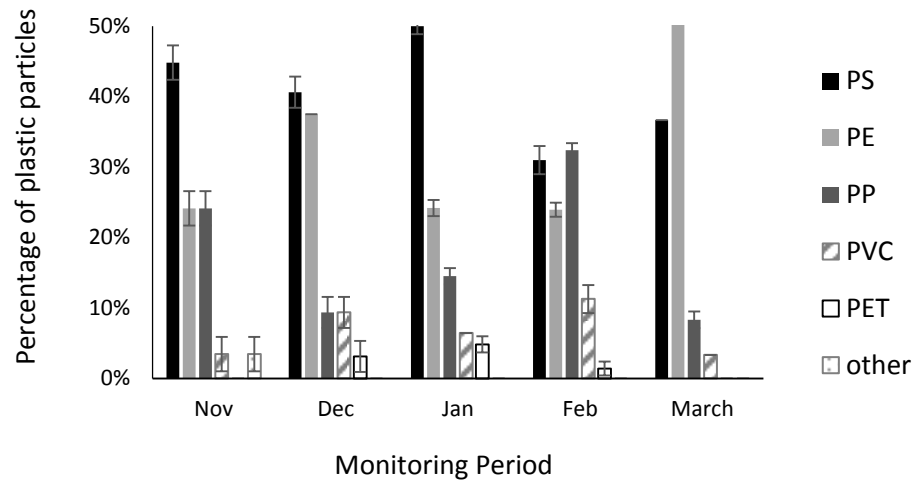
621 trajectory potentials across the local area. The source point (deposition location in a back-trajectory
622 model) was set to 43N 1E 100m a.g.l.

623 **Methodology References**

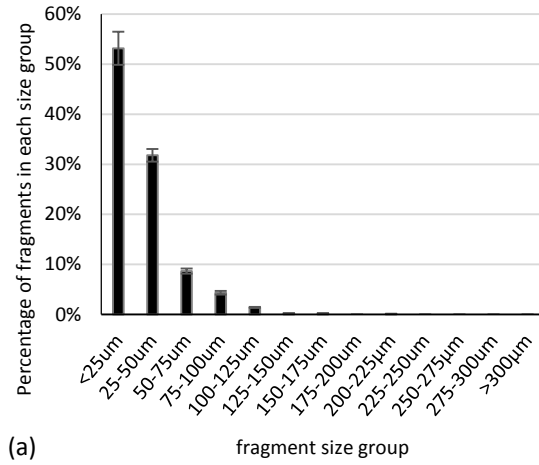
- 624 38. Digka, N., Tsangaris, C., Kaberi, H., Adamopoulou, A. & Zeri, C. Microplastic Abundance and
625 Polymer Types in a Mediterranean Environment. in *Proceedings of the International*
626 *Conference on Microplastic Pollution in the Mediterranean Sea* (eds. Cocca, M. et al.) 17–24
627 (Springer Water. Springer, Cham, 2018). doi:10.1007/978-3-319-71279-6
- 628 39. Wang, W., Ndungu, A. W., Li, Z. & Wang, J. Microplastics pollution in inland freshwaters of
629 China: A case study in urban surface waters of Wuhan, China. *Sci. Total Environ.* **575**, 1369–
630 1374 (2017).
- 631 40. Klein, R. Material Properties of Plastics. in *Laser Welding of Plastics: Materials, Processes and*
632 *Industrial Applications* 3–69 (John Wiley & Sons, 2012). doi:10.1002/9783527636969
- 633 41. Löder, M. & Gerdts, G. Methodology used for the detection and identification of microplastics
634 – a critical appraisal. in *Marine Anthropogenic Litter* (eds. Bergmann, M., Gutow, L. & Klages,
635 M.) (Springer, Cham, 2015). doi:10.1007/978-3-319-16510-3_8
- 636 42. Shim, W. J., Hong, S. H. & Eo, S. E. Identification methods in microplastic analysis: a review.
637 *Anal. Methods* **9**, 1384–1391 (2017).
- 638 43. Isobe, A., Uchida, K., Tokai, T. & Iwasaki, S. East Asian seas: A hot spot of pelagic microplastics.
639 *Mar. Pollut. Bull.* **101**, 618–623 (2015).
- 640 44. Imhof, H. K. *et al.* Pigments and plastic in limnetic ecosystems: A qualitative and quantitative
641 study on microparticles of different size classes. *Water Res.* **98**, 64–74 (2016).
- 642 45. Lenz, R., Enders, K., Stedmon, C. A., MacKenzie, D. M. A. & Nielsen, T. G. A critical assessment
643 of visual identification of marine microplastic using Raman spectroscopy for analysis

- 644 improvement. *Mar. Pollut. Bull.* **100**, 82–91 (2015).
- 645 46. Enders, K., Lenz, R., Stedmon, C. A. & Nielsen, T. G. Abundance, size and polymer composition
646 of marine microplastics $\geq 10\mu\text{m}$ in the Atlantic Ocean and their modelled vertical distribution.
647 *Mar. Pollut. Bull.* **100**, 70–81 (2015).
- 648 47. K ppler, A. *et al.* Analysis of environmental microplastics by vibrational microspectroscopy:
649 FTIR, Raman or both? *Anal Bioanal Chem* **408**, 8377–8391 (2016).
- 650 48. Song, Y. K. *et al.* A comparison of microscopic and spectroscopic identification methods for
651 analysis of microplastics in environmental samples. *Mar. Pollut. Bull.* **93**, 202–209 (2015).
- 652 49. Menges, F. Spectragryph – optical imaging software. (2016). Available at:
653 <https://www.ffmpeg2.de/spectragryph/>.
- 654 50. Khashaba, P. Y., Ali, H. R. H. & El-Wakil, M. M. A rapid Fourier transform infrared
655 spectroscopic method for analysis of certain proton pump inhibitors in binary and ternary
656 mixtures. *Spectrochim. Acta Part A Mol. Biomol. Spectrosc.* **190**, 10–14 (2018).
- 657 51.  ev ik, R. & M cov , P. Localized quantification of anhydrous calcium carbonate polymorphs
658 using micro-Raman spectroscopy. *Vib. Spectrosc.* **95**, 1–6 (2018).
- 659 52. Lagaron, J. M., Dixon, N. M., Reed, W., Pastor, J. M. & Kip, B. J. Morphological characterisation
660 of the crystalline structure of cold-drawn HDPE used as a model material for the
661 environmental stress cracking (ESC) phenomenon. *Polymer (Guildf)*. **40**, 2569–2586 (1999).
- 662 53. Draxler, R. R. & Hess, G. D. Hysplit4 modeling system. (2018).
- 663 54. Stein, A. *et al.* NOAA’s HYSPLIT atmospheric transport and dispersion modeling system. *Bull.*
664 *Am. Meteorol. Soc.* **96**, 2059–2077 (2015).
- 665 55. Su, L., Yuan, Z., Fung, J. C. H. & Lau, A. K. H. A comparison of HYSPLIT backward trajectories
666 generated from two GDAS datasets. *Sci. Total Environ.* **506–507**, 527–537 (2015).

- 667 56. Ashrafi, K., Shafiepour-Motlagh, M., Aslemand, A. & Ghader, S. Dust storm simulation over
668 Iran using HYSPLIT. *J. Environ. Heal. Sci. Eng.* **12**, 9 (2014).
- 669 57. Reche, I., D'Orta, G., Mladenov, N., Winget, D. M. & Suttle, C. A. Deposition rates of viruses
670 and bacteria above the atmospheric boundary layer. *ISME J.* (2018). doi:10.1038/s41396-017-
671 0042-4
- 672

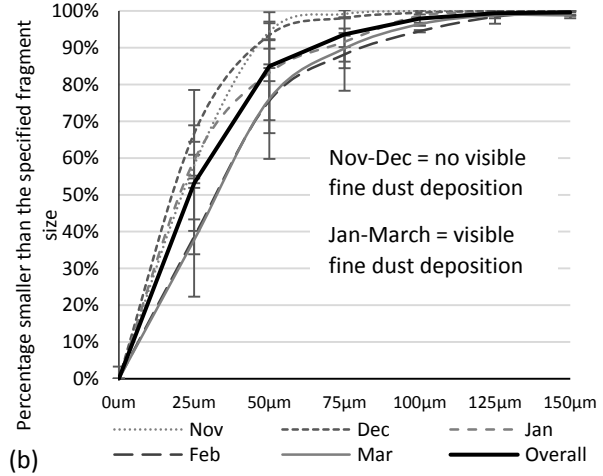


Particle size distribution of fragments in the atmospheric deposition samples



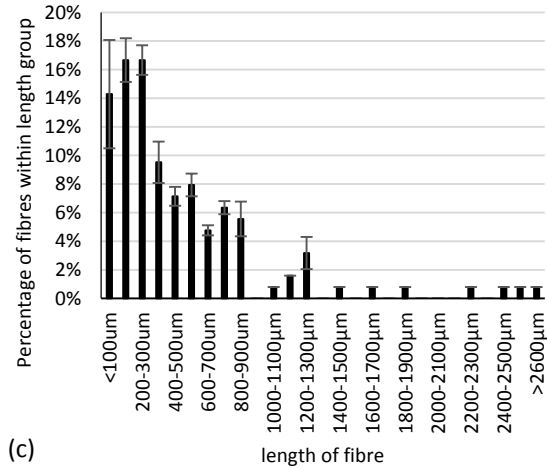
(a)

Particle size distribution by sample period



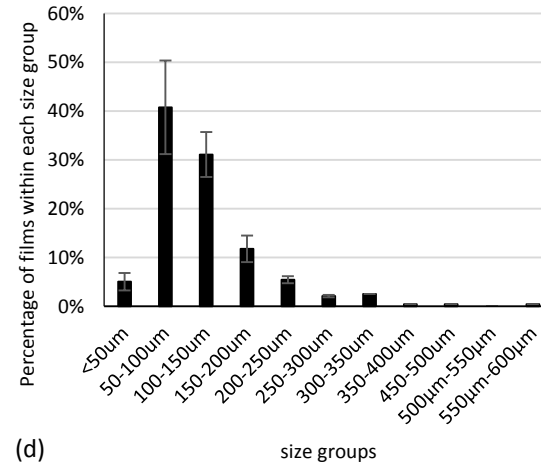
(b)

Fibre lengths



(c)

Size of films in deposition



(d)

